

Comparative study of first- and second-order Raman spectra of MWCNT at visible and infrared laser excitation

E.F. Antunes^{a,*}, A.O. Lobo^{a,b}, E.J. Corat^{a,*}, V.J. Trava-Airoldi^a,
A.A. Martin^b, C. Veríssimo^c

^a *Associated Laboratory for Sensors and Materials (LAS), National Institute for Space Research (INPE), CP515 – São José dos Campos/SP 12.245-970, Brazil*

^b *Laboratory of Biomedical Vibrational Spectroscopy, University of Vale do Paraíba (UNIVAP), Av. Shishima Hifumi, 2911– São José dos Campos/SP 12.244-000, Brazil*

^c *Center of Semiconductor Components (CCSUNICAMP), CP6061, Campinas/SP 13.083-970, Brazil*

Received 31 May 2005; accepted 3 March 2006

Available online 18 April 2006

Abstract

Comparative studies of first- and second-order Raman spectra of multi-walled carbon nanotubes (MWCNT) and three other graphitic materials – carbon fiber, powdered graphite and highly ordered pyrolytic graphite – are reported. Three laser excitation wavelengths were used: 514.5, 785 and 1064 nm. In first-order Raman spectra, the positions of the bands D, G and D' ($1100\text{--}1700\text{ cm}^{-1}$) presented very similar behavior, however the intensity (I) ratio I_D/I_G ratio showed differed behaviors for each material which may be correlated to differences in their structural ordering. In the second-order spectra, the G' band varied strongly according to structure with the infrared laser excitation.

© 2006 Elsevier Ltd. All rights reserved.

Keywords: Carbon nanotubes; Graphite; Carbon fiber; HOPG; Raman spectroscopy

1. Introduction

Raman spectroscopy is an analytical technique largely used for characterization of different carbon based materials, either graphite-like or diamond-like. The great versatility of carbon materials arises from the strong dependence of their physical properties on the ratio of sp^2 (graphite-like) to sp^3 (diamond-like bonds). There are many forms of sp^2 -bonded carbons with various degrees of graphitic ordering, ranging from single crystals of graphite, nanocrystals to glassy carbon. Moreover, there is a full range of amorphous carbons [1,2].

Raman spectroscopy of carbon nanotubes has attracted a lot of attention in recent years, both theoretically and experimentally. Theoretically, it is possible to predict mor-

phological characteristics such as the diameter of the tubes or their conductance properties, especially of single wall carbon nanotubes (SWCNT) [3]. Experimentally, it is a powerful method for determining the degree of structural ordering or presence of contaminants [4,5].

Multi-walled carbon nanotubes (MWCNT) are made of concentric graphene sheets rolled in a cylindrical form with diameters of tens of nanometers. In first-order Raman spectra, all graphite-like materials, including MWCNT, show, a strong peak around 1580 cm^{-1} (G), which is the high-frequency E_{2g} first-order mode; an additional band around 1350 cm^{-1} (D); and a weak band around 1620 cm^{-1} (D'), using laser excitation of 514.5 nm [6–8]. In the second-order Raman spectra, the main lines are 2450 cm^{-1} , 2705 cm^{-1} (G'), 2945 cm^{-1} (D+G), 3176 cm^{-1} (2G), and 3244 cm^{-1} (2D') at 514.5 nm excitation [9–11].

Previous studies using multiple excitation wavelengths have revealed that the G peak does not disperse in graphite itself, nanocrystalline graphite, or glassy carbon. The G

* Corresponding authors. Tel.: +55 12 3945 6576; fax: +55 12 3945 6717.
E-mail addresses: ericafa@las.inpe.br (E.F. Antunes), corat@las.inpe.br (E.J. Corat).

peak only disperses in more disordered carbon, where the dispersion is proportional to the degree of disorder. The G peak in graphite cannot disperse because it is the Raman-active phonon mode of the crystal [1]. Another important feature of the Raman spectra is associated with the disorder-induced D band, as follows: (i) the laser wavelength dependence of D band position is essentially independent of the type of graphitic material involved; (ii) for graphitic materials the frequency of the D band shifts upward with increasing of laser excitation energy [1,12–15]. Raman spectra of aligned carbon nanotubes usually have very strong D line [16].

Calculations carried out for graphite, using group theory, predicts only the origin of the G band as a first-order Raman scattering. D and D' have their origin explained by the double resonance theory [17–19]. In double resonance processes, the origin of the D band and the many weak dispersive phonon modes in the Raman spectra of graphite are explained by resonant enhancement of Raman intensity in two consecutive scattering processes. Basically, an electron with momentum k is (a) first excited to the energy $E_i(\mathbf{k})$ by the incident photon, (b) scattered to a state $\mathbf{k} + \mathbf{q}$ [$E(\mathbf{k} + \mathbf{q})$] and then (c) backscattered to state k [$E_f(\mathbf{k})$], and finally, (d) recombined with a hole to yield the scattered photon. If $E(\mathbf{k} = \mathbf{q})$ and either the $E_i(\mathbf{k})$ or $E_f(\mathbf{k})$ states correspond to real electronic states, the Raman intensity is enhanced by two resonant factors in the denominators occurring in the intensity formula, and this is known as the double-resonance Raman. In double resonance Raman processes in bi-dimensional Brillouin zone of graphite, the electrons around the K point are relevant to Raman processes [20]. The electron wave vector \mathbf{k} and the phonon wave vector \mathbf{q} increase if laser energy increases. Because this, the frequency of D band changes, or either, phonon branch is dispersive. D' band is due to the same process, but it arises close Γ point in Brillouin Zone [20,2,22]. The position of most lines in second-order Raman spectra are also explained by the double resonance theory, due to combinations or overtones of the first-order modes.

Even though the double resonance theory is able to explain the dispersive behavior of most bands correctly, the behavior of their intensities and their dependence on energy of excitation laser are not so clear.

In this study, we have studied Raman spectra of MWCNT. Three other graphitic materials were used for comparison – carbon fibers, powdered graphite, and HOPG. We have investigated spectra of aligned carbon nanotubes produced by microwave plasma and nanotubes grown by thermal processes. Three different Raman systems were used with laser in visible (514.5 nm) and infrared (785 and 1064 nm) regions. The results confirm the dispersive behavior of first- and second-order Raman bands for all materials studied. However, each material showed a different variation of band intensities with laser wavelength. In particular, defects in graphitic structure are very sensitive to infrared excitation, producing pronounced variation in the intensity of bands D and G'.

2. Experimental

Two different types of carbon nanotubes were obtained. The samples of nanotubes, called “CNT1”, were produced at CCS/UNICAMP on silicon wafer substrates covered by a 50 nm thick SiO_2 diffusion barrier. A 6 nm thick Ni catalyst film was deposited by electron beam evaporation. The substrate-supported catalyst was annealed in a quartz tube furnace at 700 °C in 1 mbar of N_2/H_2 , with RF plasma cleaning during 15 min. Ni nanoparticles formed, a flow of 400 sccm of H_2 was opened to fill the chamber up to atmospheric pressure, and the temperature was rapidly increased to 900 °C. At the initial stage of growth, H_2 was replaced by a flow of 400 sccm of NH_3 , and CH_4 was introduced (100 sccm). After the first 5 min of the addition of CH_4 , the NH_3 was replaced by H_2 (400 sccm). The total growth time was 30 min [23].

The other samples of nanotubes, called “CNT2”, were produced in thin film form in a microwave plasma chamber built at INPE. Silicon was used as the substrate, covered by a layer of 50 nm of SiO_2 . A thin (5 nm) nickel layer deposited by an e-beam evaporator was used as catalyst. The nickel layer was pre-treated to promote nanoclusters formation and the nanotubes nucleate from them. The pre-treatment was carried out during 5 min in N_2/H_2 plasma at a substrate temperature of 700 °C. After pre-treatment, CH_4 was added to the gas mixture as a carbon source. The nanotubes growth was performed during 2 min at a temperature of 750 °C. The gas flow was N_2 : 10 sccm, H_2 : 90 sccm and CH_4 : 14 sccm, respectively. The reactor was kept at a pressure of 30 Torr during the whole process. External heating with a Ni–Cr resistance under the substrate holder was necessary to maintain the substrate temperature.

As comparative materials, we used carbon fibers, powdered graphite and highly ordered pyrolytic graphite (HOPG). Carbon fibers were produced from fibers of polyacrylonitrile (PAN). The temperature used to treat the fibers was 2000 °C by using the temperature steps of 60 °C/h in a nitrogen atmosphere up to 1000 °C and for more 4 h up to 2000 °C. The samples consisted of 0.15 cm thick with a diameter of 1.8 cm. The powdered graphite was obtained by grinding good quality commercial graphite of Carbono Lorena Ltda.

Scanning electron microscopy (SEM) was performed with a FEG-SEM JSM6330 and transmission electron microscopy was performed with a HITACHI HG000-NA.

Raman spectroscopy was used to analyse the structure of these samples. Three Raman spectrometers were used, as follows: (a) a Renishaw micro-Raman, model 2000, with Argon laser (514.5 nm); (b) a home mounted system composed of a Ti-Safire laser, tuned at 785 nm (Spectra Physics 3900 s), pumped by an Argon laser (Spectra Physics 2017 at 514.5 nm) and (c) a FT-Raman Bruker/RF100 with Nd:YAG laser (1064 nm).

3. Results and discussion

The CNT1 samples were long nanotubes randomly distributed on the surface, as shown in Fig. 1(a). The nanotubes in CNT2 grew roughly perpendicular to the substrate, forming a dense forest of aligned nanotubes, as

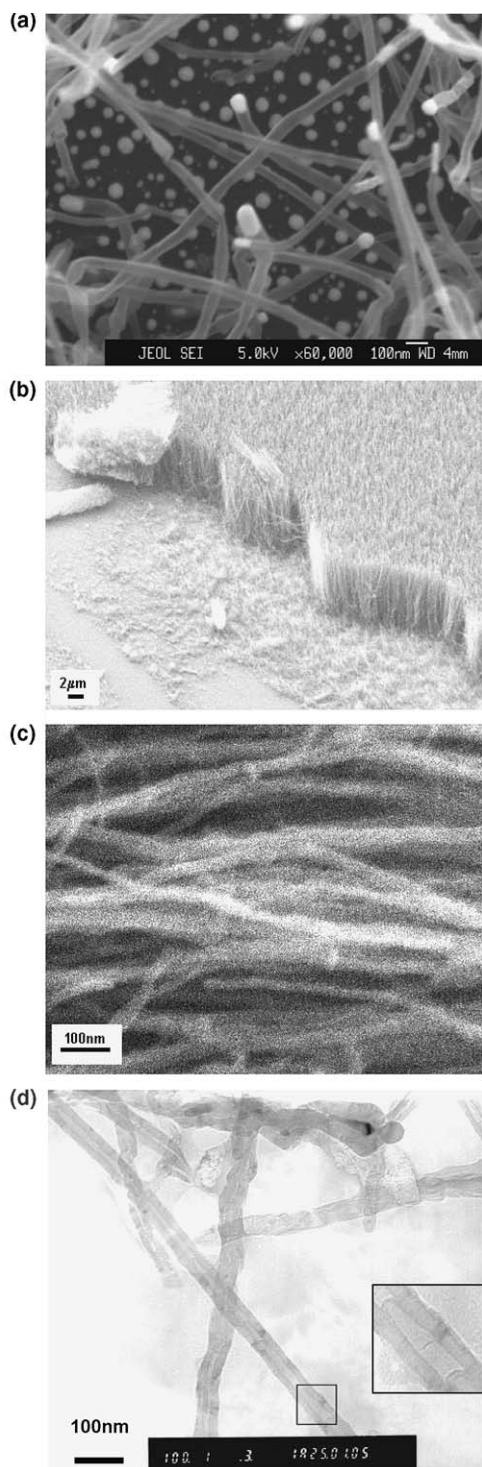


Fig. 1. (a) CNT1 – magnification: 60,000×; (b) CNT2 – magnification: 5000×; (c) CNT2 – magnification: 120,000× and (d) TEM image of some nanotubes of CNT2.

shown in Fig. 1(b). Fig. 1(c) is a higher magnification of Fig. 1(b). Fig. 1(d) is a TEM image of CNT2. Both CNT1 and CNT2 are multi-walled with 30–80 nm external diameter.

3.1. First-order spectra

Fig. 2(I) shows first-order Raman spectra obtained for HOPG, graphite, carbon fibers and carbon nanotubes. The HOPG shows only the G band at visible laser excitation and only a very small intensity D band with infrared excitation. Graphite, carbon fibers and carbon nanotubes have very similar Raman spectra. All of them show the D, G and D' bands. In particular, a small shoulder at the left of the D band was observed with 1064 nm excitation for CNT2. The origin of G, D and D' have been already explained by other authors [24], but the shoulder's origin has not been as clearly identified. Probably the shoulder has its origin in double resonance process, because its Raman shift ($\sim 1200 \text{ cm}^{-1}$) is a point on phonon dispersion curves. The band at 1200 cm^{-1} can be attributed to iTA, LA or LO modes very close to the K point, or a convolution of them [2,21].

3.1.1. Deconvolution of first-order bands

An overall observation of these spectra shows that the D band downshifts with increasing wavelength and its relative intensity increases; the G band position is marked by the dotted line as reference. The increase of the relative intensity of the D' band looks as if G band have upshifted with increasing wavelength. However, a closer observation is shown in Figs. 3(a1)–(b1) and 4(a1)–(b1), with the deconvolution on the G and D' bands. Notice that the D' band may become much larger than the G band for excitation wavelengths in infrared region. For the curve fitting, we have used Lorentzian shapes for D and G band, and Gaussian shape for D' one, as proposed by Mennela [11]. This fitting alternative always resulted in a natural convergence with no dispersion of G band. Other fitting alternatives always resulted in the upshift of G band for laser excitation in the infrared. Since many authors agree that G band is non-dispersive for graphitic materials this is an adequate curve fitting alternative.

The increase of relative intensities of the D and D' bands (I_D/I_G and $I_{D'}/I_G$) with infrared excitation has already been observed by other authors [25] and is related to a larger electron–phonon interaction for D and D' bands with respect to G peak, as described by double resonance theory [26].

3.1.2. Evaluation of band intensities

In Fig. 5 the positions of each peak are plotted for the three excitation wavelengths. Clearly, the G band position is relatively constant for graphite-like materials excited at different wavelengths, while the D band position changes drastically (around 70 cm^{-1}), with about the same dispersion behavior for all of the materials tested. The D' band

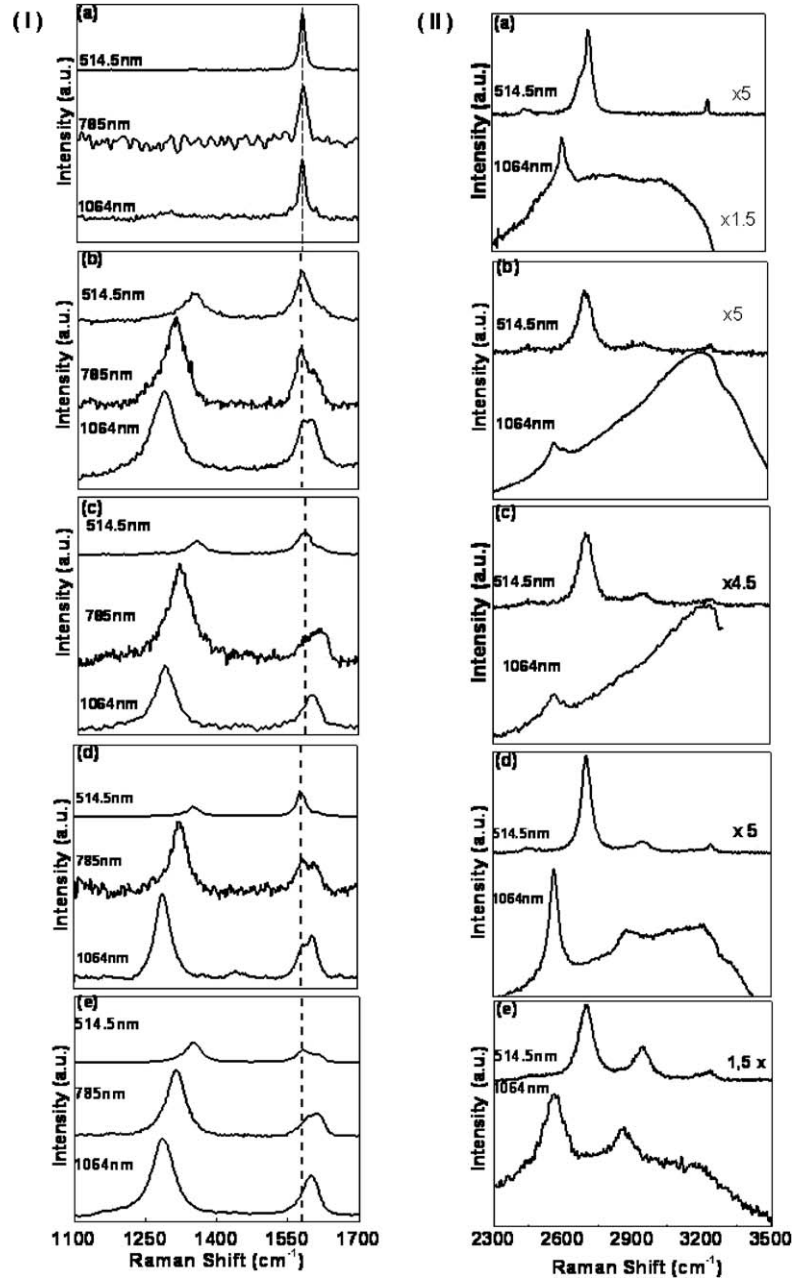


Fig. 2. (I) First-order Raman spectra (normalized by G peak) of (a) HOPG, (b) Powdered Graphite, (c) Carbon Fiber, (d) CNT1 and (e) CNT2, using three excitation wavelengths (514.5, 785 and 1064 nm). (II) Second-order Raman spectra (normalized by G peak) of (a) HOPG, (b) Powdered Graphite, (c) Carbon Fiber, (d) CNT1 and (e) CNT2, using two excitation wavelengths (514.5 and 1064 nm). The G band position is marked by the dotted line as reference.

is also dispersive, but with a smaller trend (around 20 cm^{-1}) than the D band. These observations are in agreement with the observations of Wang et al. [6] for other graphitic materials. The presence of G and the dispersive behaviors of D and D' bands, together with relatively low values of linewidths ($20\text{--}40 \text{ cm}^{-1}$) indicate a high degree of graphitization of all materials.

Fig. 6 shows the graphs of relative intensities of the D and G bands (I_D/I_G) for the different wavelengths. The I_D/I_G ratio increases for infrared wavelengths for all of the graphitic materials tested. However, the behavior is

different for each material. Graphite presents smaller values for I_D/I_G and a smaller trend with the increase of the wavelength. The CNT1 and carbon fiber have around the same value of graphite at 514.5 nm but the trends with increasing wavelength are larger. The slope of I_D/I_G curve for carbon fiber is larger than for CNT1. The CNT2 has much larger values than graphite and has the largest slope. It is very important to reaffirm the great enhancement of D band relative to G band with infrared excitation, which is responsible for the high values of I_D/I_G , around 6 for CNT2.

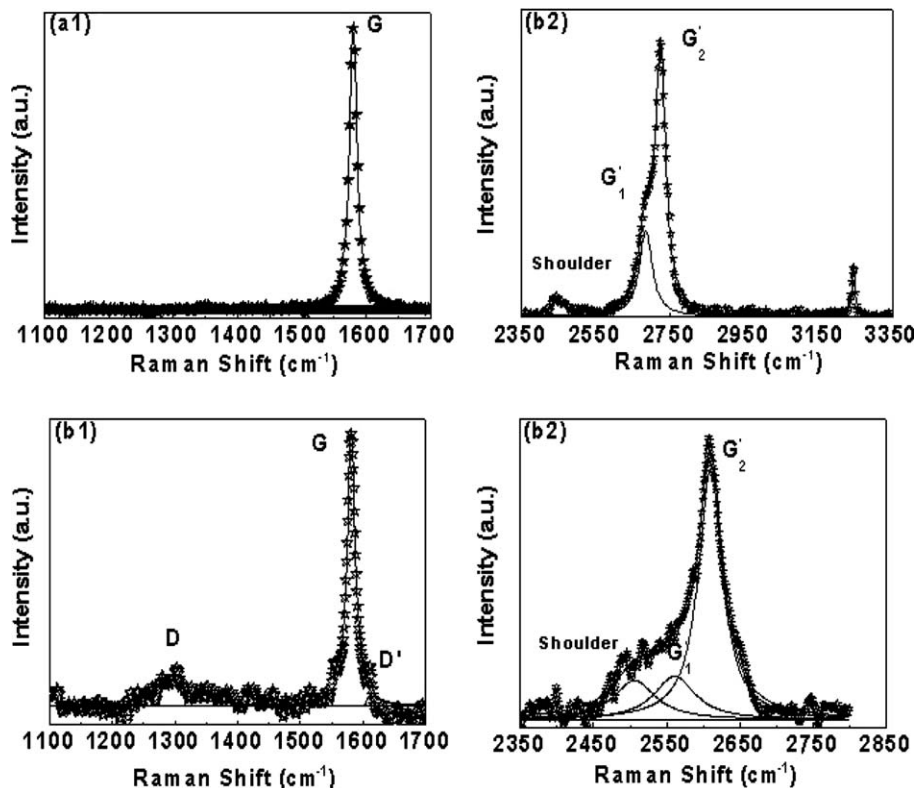


Fig. 3. HOPG: (a1) D and G Band at 514.5 nm; (a2) 2G band, a shoulder and the deconvolution of G1'e G2' bands at 514.5 nm; (b1) D band and the deconvolution of G and D' bands at 1064 nm; in this case D' is very low; (b2) Deconvolution of a shoulder, G1' and G2' bands at 1064 nm.

Fig. 7 shows the graph of $I_{D'}/I_D$ as a function of the excitation wavelength for the five materials. This ratio increases with the increase of wavelength for all of the materials tested. The trends are very similar for all materials, indicating that D and D' bands have the same origin as predicted by the double resonance theory. The $I_{D'}/I_D$ increase with the increase of wavelength excitation can be understood as a slightly relative decrease in the density of (k, q) pairs [22], which generate the phonon modes around K and Γ points.

The I_D/I_G ratio has been used to correlate the structural purity of graphitic materials to the graphite crystal domain size [8], as obtained by X-ray diffraction [27]. The intensity of the D band is considered defect dependent. According to the double resonance theory the crystal defects scatters the excited electrons resulting in the wave vector condition, which explain the D band's appearance. In principle, the larger the number of defects, the higher the D band intensity.

The double resonance theory explains the dispersive behavior very well. However, the only insight it gives to band intensity dependence on energy of excitation laser is based on the phonon wave vector condition for double resonance ($q \sim 2k$, around the K point), which for lower energies give a condition closer to the equality ($q = 2k$) and a stronger resonance. This may explain the fact that the I_D/I_G ratio increases for longer wavelengths, but the theory does not predict how much it will increase.

The results obtained in this study generically confirm these assumptions: graphite has a higher degree of crystalline order, while carbon fiber and MWCNT have more structural defects, and the I_D/I_G ratio increases with the increase of laser wavelength. However, the trend is different for each of the materials tested.

Some authors report the importance of crystallites size. Ferrari and Robertson [1] observed that, in graphitic materials with smaller crystallites (nanocrystalline compared to micro-crystalline graphite) the increment in I_D/I_G is greater for large wavelengths. Castiglioni et al. [28] presented a formulation, alternative to double resonance theory, to explain Raman spectra of graphitic materials, based on the correlation of sp^2 domains with PAH molecules of different sizes. In their formulation, the distribution of sp^2 domains of different size and shape imply a distribution of excitation energies (energy gaps) of allowed localized electronic states, which may have an influence in determining the shape and the maximum frequency of D band.

Our results support the findings of Ferrari and Robertson [1] observation. The CNT2 has smaller sp^2 domains than carbon fibers, which had smaller sp^2 domains than CNT1 which had smaller sp^2 domains than graphite, which had smaller sp^2 domain than HOPG, as shown by the increase in the I_D/I_G ratio. The smaller sp^2 domains also suggest a larger trend with wavelength. However, the observation only at 514.5 nm indicates a similar defect density or sp^2 domain size in graphite, carbon fiber, and

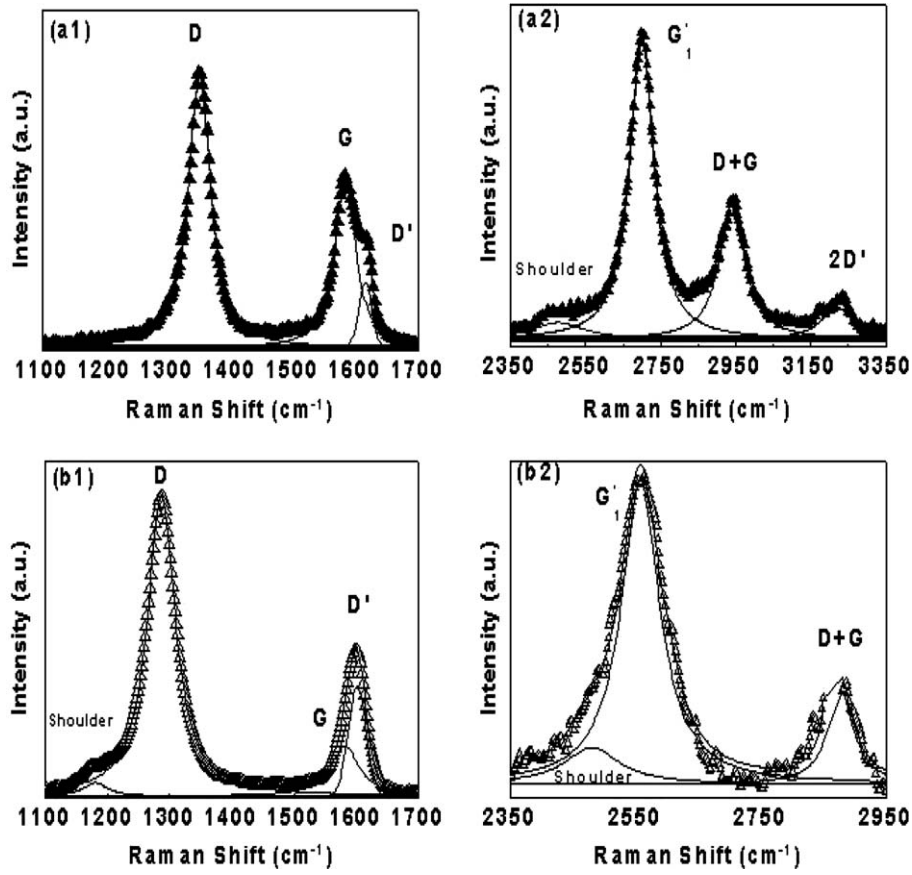


Fig. 4. CNT2: (a1) D band and deconvolution of G and D' bands at 514.5 nm; (a2) deconvolution of a shoulder, G₁', D+G, and 2D' at 514.5 nm – in this case, the intensity of G₂' is very low; (b1) D band and deconvolution of G and D' bands at 1064 nm and (b2). D+G band and the deconvolution of a shoulder and G₁' bands at 1064 nm.

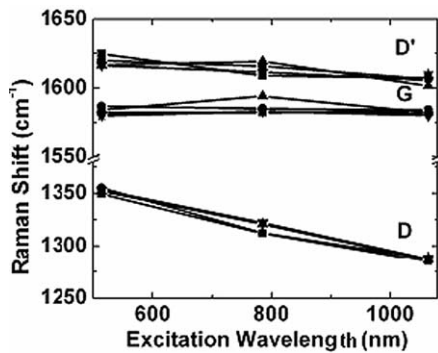


Fig. 5. Band position. Legend: (★) HOPG, (■) powdered graphite, (●) carbon fiber, (▼) CNT1, (▲) CNT2.

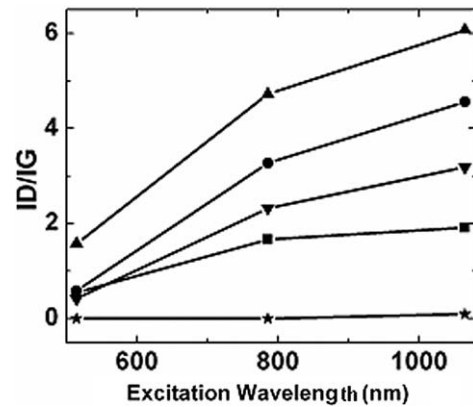


Fig. 6. ID/IG. Legend: (★) HOPG, (■) powdered graphite, (●) carbon fiber, (▼) CNT1, (▲) CNT2.

CNT1, while the observation at longer wavelengths indicates greater defect density and smaller sp^2 domain size in CNT1 and carbon fiber than in graphite powder. Fig. 6 suggests a crossing point for these three materials in the visible region.

The I_D/I_G ratio obtained with laser excitation in the visible region is commonly used to determine the degree of graphitization of carbon fibers ($L_a \cdot I_D/I_G = 43.5$, where L_a is the dimension of the basic sp^2 structural unit of the carbon fiber) [29]. However, there are no known studies

of PAN carbon fibers with Raman spectra excited in the infrared, as shown in this study. Recently Lee [27] found discrepancies in the evaluation of L_a by first-order Raman spectra (excitation at 488 nm), compared with X-ray diffraction. He observed that L_a was overestimated and I_D/I_G was relatively insensitive to structure variation. He proposed the use of second-order Raman spectra as a better

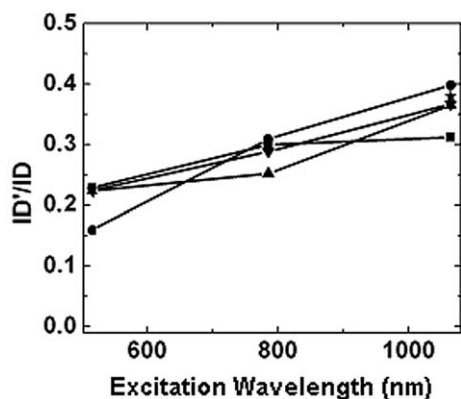


Fig. 7. $I_{D'}/I_D$. Legend: (★) HOPG, (■) powdered graphite, (●) carbon fiber, (▼) CNT1, (▲) CNT2.

alternative, using the comparison of G' band intensity and line broadening.

Tan et al. [30] have shown a new type of graphite whiskers in which the I_D/I_G ratio is clearly not associated with the crystallite size and have suggested that there may be a special enhancement factor of the D mode, probably associated to the brim structure of the whiskers.

Recently, Barros et al. [31] presented an interesting Raman study on different regions of graphitic foam that show different I_D/I_G ratios. They correlated these differences to structures of 2D and 3D graphite present in the foam. 2D graphite is interpreted as individual graphene sheets, or a structure of non-aligned and unevenly spaced graphene sheets. 3D graphite is interpreted as a structure of well aligned and evenly spaced graphene sheets. They suggest that the 2D graphite structure enhances D band intensity.

A good revision of the doublet structure observed in the D band was presented by Tan et al. [32]. This doublet is characteristic of graphite edge planes and has been related to the coupling between well aligned and evenly spaced graphene sheets (3D graphite). In this doublet, the lowest energy peak has been considered as a typical feature of the edge plane, while the highest energy is the one related to the number of defects [33].

All these observations [27,30–33] indicate that the correlation of I_D/I_G ratio with domain size may be considered a first approach and that there is some influence of structural arrangement on the enhancement of the D band relative to the G band.

In the observations presented here it is interesting to note the different structural arrangements of each material tested: HOPG is a long range 3D structure which is observed on its basal plane; graphite powder is of micrometric range, obtained from a good quality polycrystalline graphite and its Raman spectra should have a great contribution from steps and edge planes; carbon fiber is highly graphitized but still with some turbostratic structure, which should give some contribution from 2D graphite to the Raman spectra; CNT1 are long nanotubes with little defect

density along its axis, and; CNT2 samples are analyzed from the top surface and the major contribution to the Raman spectra is from the domed tips of the aligned nanotubes. The comparison of materials of different structural arrangements, as shown here, indicates that not only the domain size, but also the kind of defect or defect arrangement, may be responsible for the different trend shown in I_D/I_G ratios.

3.2. Second-order spectra

Fig. 2(II) shows the second-order Raman spectra for HOPG, graphite, carbon fiber and carbon nanotubes with excitation at 514.5 and 1064 nm. All the spectra have been normalized to the intensity of the G band ($\sim 1584 \text{ cm}^{-1}$) of each spectrum. The spectra at 1064 nm excitation are always superimposed on a fluorescence background due to infrared heating of the samples. This background prevents a precise analysis of the $2D'$ band around 3200 cm^{-1} at 1064 nm excitation. All other bands in this region of the spectrum were analyzed by proper subtraction of the background, deconvolution of the bands, and normalization to the G band intensity of each spectrum. We have used Lorentzian shapes for the curve fitting.

The analyses of HOPG and CNT2 are presented in Figs. 3(a2) and (b2) and 4(a2) and (b2), respectively, as characteristic examples of the deconvolution of the bands. The $G1'$ and $G2'$ bands and a non-assigned shoulder is the set of bands of more difficult identification. The analysis of the other bands is straightforward. The $G1'$ and $G2'$ bands are fundamental for analyzing the behavior of each graphitic material. We can notice that HOPG has a $G2'$ of higher intensity while the CNT1 has only the $G1'$ band.

Fig. 8 summarizes the behavior of all Raman bands, both first and second order. All intensities are normalized

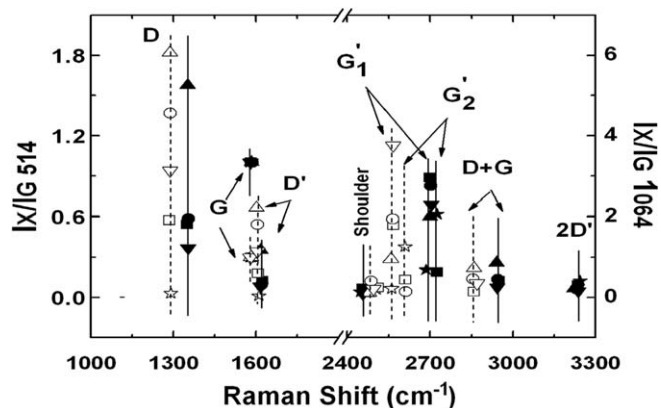


Fig. 8. Relative intensities of peaks: first-order peaks ($X = D, G$ and D') and second-order peaks ($X = \text{shoulder}, G1', G2', D+G$ and $2D'$) for each carbon material using two excitation wavelengths (514.5 and 1064 nm). Legend – 514.5 nm: (★) HOPG, (■) powdered graphite, (●) carbon fiber, (▼) CNT1, (▲) CNT2; 1064 nm: (☆) HOPG, (□) powdered graphite, (○) carbon fiber, (▽) CNT1, (△) CNT2.

to the G band intensity of each spectrum. The solid symbols and solid lines correspond to 514.5 nm excitation. The open symbols and dashed lines correspond to excitation at 1064 nm. The scale for the relative intensities obtained at 514.5 nm (left scale) is 30% of the scale of band intensities obtained at 1064 nm (right scale), which indicates that all bands have higher intensity relative to the G band with the excitation in the infrared region. The first-order bands are included for comparison.

The second-order Raman spectrum of HOPG with 514.5 nm excitation shows a shoulder at 2450 cm^{-1} , the G' band, with the characteristic G1' (2685 cm^{-1}) and G2' (2725 cm^{-1}), and the 2D' (3245 cm^{-1}) band. Weaker bands were not analyzed. With 1064 nm excitation, the G1' and G2' bands shifted to 2560 and 2610 cm^{-1} , respectively.

The other materials tested also presented a shoulder and G', besides D+G and 2D' bands. D+G band occurred at around 2950 cm^{-1} , and the 2D' band was found out around 3230 cm^{-1} , under visible excitation. D+G downshifted to 2870 cm^{-1} under infrared excitation. The 2D' band was not analyzed with the infrared laser because of the thermal background.

The 2450 cm^{-1} band was assigned by Tan et al. [34] as the T+D band which has a negative dispersion, where T is a band that appears at around 1083 cm^{-1} , for visible excitation wavelength. Shimada et al. [35] reported that the 2450 cm^{-1} band did not show any dispersion and should be characterized as the overtone mode of a LO phonon near the K point. We, however, found this band to be dispersive. With excitation at 1064 nm, the shoulder dispersed up to 2510 cm^{-1} and the intensities were about the same for all materials tested. The dispersion of this shoulder band was to larger wavenumbers (negative dispersion). With excitation in the infrared region this dispersion is very clear. It is interesting to notice that the dispersion varies slightly among the different materials. Recently, the origin of the 2450 cm^{-1} shoulder has been described as an overtone of the band around 1200 cm^{-1} (iTA, LA or LO modes very close to the K point or a convolution of them). The observation of the dispersion of this band is very important, because it may disclose its origin since each of the modes has its dispersion predicted. However, one can notice that the dispersion observed in our study is larger than previous theoretical values for the dispersion in these phonon branches [21].

The intensities of the 2D' band are also similar for all of the materials tested. The intensities of the D+G bands are lower than the D band intensity, but the relative intensities among the different materials follow the same behavior as the D band. Also, the dispersion of the D+G band is similar to the dispersion of the D band. These three bands (shoulder, D+G and 2D') do not help to distinguish between graphitic materials because the shoulder and 2D' bands appear to be independent of the material (or at least their intensities are too small to account for variations in their values) and the D+G band brings similar information of the D band.

In contrast, the G1' and G2' bands showed variation among the material tested. HOPG showed the usual two peaks at 2685 and 2725 cm^{-1} at 514.5 nm , which shifted to 2560 and 2610 cm^{-1} at 1064 nm . The ratio of their intensities ($I_{G1'}/I_{G2'}$) is smaller than 1 and of the same order of magnitude, regardless of the excitation wavelength (0.33 at 514.5 nm and 0.18 at 1064 nm). The powdered graphite also presented both bands at 2700 and 2725 cm^{-1} ($I_{G1'}/I_{G2'} = 4.7$) with excitation at 514.5 nm and, at 2566 and 2610 cm^{-1} ($I_{G1'}/I_{G2'} = 4.1$) with excitation at 1064 nm . The carbon fiber at 514 nm showed G1' and G2' at approximately the same wavenumbers of graphite, but with larger $I_{G1'}/I_{G2'}$ intensity ratio (5.6). At 1064 nm the presence of G2' is not as clear. The fitting naturally finds a band around 2610 cm^{-1} but the $I_{G1'}/I_{G2'}$ is larger than 13. Therefore, we assigned only the G1' band (2565 cm^{-1}) for carbon fiber with excitation at 1064 nm . For both carbon nanotube samples (CNT1 and CNT2) only the G1' band was observed at around 2700 and 2560 cm^{-1} for excitation at 514.5 and 1064 nm , respectively.

Similarly, $I_{G1'}/I_G$ ratios also differed. Powdered graphite and carbon fiber had similar values at each of both excitation wavelengths (~ 0.8 at 514.5 nm and ~ 1.8 at 1064 nm). Both carbon nanotubes samples presented similar values for 514.5 nm excitation ($I_{G1'}/I_G \sim 0.6$), but the behavior at 1064 nm excitation is very dissimilar. The CNT1 sample has the high value of $I_{G1'}/I_G = 3.75$ while for the CNT2 sample the $I_{G1'}/I_G$ ratio increased only to 0.95.

The G' band has origin in double resonance process, as the D band, but it does not present conservation constraint, because it is a second-order Raman feature that involves two phonons with wave vectors q and $-q$. In other words, the elastic phonon scattering responsible for the appearance of the D band in the presence of lattice defects is replaced by an inelastic phonon emission process for G' band.

The G' band splitting into the G1' and G2' bands has been observed by many authors. Mennella et al. [11] attributed G2' to the density of states peaks and G1' to the interaction with boundary phonon, which is also responsible for the D band. Nemanich and Solin [8] clearly showed the dominance of the G2' band for samples of larger crystallites, while G1' band dominates in samples of smaller crystallites.

In the study of Barros et al. [31], the G' band is thought to be formed by three peaks, two due to 3D graphite and one due to 2D graphite. A triplet G' band has also been observed in the edge plane of graphite crystals by Tan et al. [34]. Barros et al. [31] found a correlation between the increase of the G' peak due to 2D graphite and the increase of the D band in graphitic foam. The 3D graphite peaks are correspondent to the G1' and G2' of HOPG (2685 and 2725 cm^{-1} at 514.5 nm) and the 2D graphite peak is correspondent to the G1' band of the other graphitic materials (2700 cm^{-1} at 514.5 nm), as found in our study. From this point of view, the structure of the

graphitic materials presented in our study may be interpreted qualitatively, as observed by the G' band: HOPG is a 3D graphite material; the powdered graphite present a major contribution of 2D graphite but still holds some contribution from 3D graphite ($I_{G'}/I_{G''}$ is around 4 for both wavelengths); the partially turbostratic structure of carbon fiber presents major contribution of 2D graphite and the contribution of 3D graphite is smaller than in powdered graphite; CNT1 and CNT2 are essentially 2D graphitic materials.

The observed variation of $I_{G'}/I_G$ ratio of both carbon nanotubes (CNT1 and CNT2) may reflect the difference in their structures. Besides the fact that both are MWCNTs with similar diameter, the CNT1 have a low density of long tubes with little defect density along their axis, while CNT2 contained a high density of short nanotubes with high defect density. Variations may be due to different analysis procedure. For CNT1 the laser probes the lateral of the tubes. For CNT2, the laser probes the tips of the tubes where there is a larger concentration of defects. The characteristics of the sample are also reflected in the linewidth of the bands. CNT1 had the smallest linewidth of all samples (except the HOPG), while CNT2 present the broadest features. The smaller linewidths indicate that the CNT1 samples had a narrower distribution of defects while the broader linewidth indicate that CNT2 had a broader distribution of defects.

Tan et al. [30] observed an enormously high intensity G' band in their new graphite whiskers, but they attributed this effect to the particular structure of the brim region where there is a curved termination of the graphite sheets that eliminate most dangling bonds. They also compared their observation to the observation of Gogotsi et al. [36] on their graphite polyhedral crystals, in which the G' band intensity is also relatively high and the structure also presented a curved termination. Dong et al. [37] explained the observations of G' on graphite whiskers by a high density of phonon states favorable to a multi-phonon process, due to disclination in whiskers.

Metallic single walled carbon nanotubes also used to present high intensity G' band. The explanation for this is based on resonances with van Hove singularities [18].

The high intensity of G' band observed in the CNT1 samples is clearly dependent on the laser excitation wavelength, since it is observed only in the infrared region. It may not be correlated with the observation of Tan et al. [30] since their observation did not depend on the excitation wavelength (from 488 to 632 nm). Further theoretical work is necessary to account for the high intensity of G' band observed in this study.

4. Conclusions

Graphitic-like materials show Raman spectra with very similar behavior, when excited by visible and infrared wavelengths, but the bands originated in the double reso-

nance process are seen with much larger efficiency in the infrared region.

In first-order Raman spectra, the G peak has its position independent of excitation wavelengths, while the D band is strongly dispersive ($\sim 50 \text{ cm}^{-1}/\text{eV}$) and the D' band present a slighter dispersion ($\sim 12 \text{ cm}^{-1}/\text{eV}$). These phenomena have already been explained by double resonance theory. However, we have observed that each graphitic material has a specific increment (slope) on I_D/I_G , which shows that relative intensities can bring further information about the presence of defects. Some graphitic materials (CNT1, powdered graphite and carbon fiber) show about the same I_D/I_G when excited by visible wavelengths, but have quite different values when infrared wavelengths are used. In principle, the trend of I_D/I_G ratio with laser wavelength excitation is larger for the materials with smaller crystallite size, but the results suggest that the structural arrangement or defects of different origins also influence them.

In second-order Raman spectra, the main peak is the G'. HOPG shows it split in two peaks, G1' and G2', while the other materials presented a convolution of G1' and G2' or just G1'. In particular, CNT2 and CNT1 presented only G1'. Although the origin of the G' band does not depend on structural defects, our experimental data show that its intensity is dependent on them, particularly for infrared laser excitation. All material presented similar behavior for $I_{G'}/I_G$ ratio, using infrared and visible wavelengths, except CNT1, which presented a very high value (3.75).

The small linewidth observed in CNT1 sample indicates that they are representative of MWCNT of very good structural order. This probably contributes to the observation of the enhancement of the G' band, because in broader features the effect would be masked.

The similarities between MWCNT first- and second-order Raman spectra with other graphitic materials make it difficult to distinguish among them. However, both I_D/I_G ratio and the $I_{G'}/I_G$ ratio at infrared excitation wavelength (1064 nm) vary according to structural order. The high enhancement of structure defects makes the infrared excitation a great alternative for the Raman study of graphitic materials.

Acknowledgements

The authors thank FAPESP for financial support, LNLS (Campinas/SP) for SEM microscopy support, M. Vila E and M.C. Ferro from Universidade de Aveiro for TEM images, A.F. Beloto (LAS/INPE) for nickel deposition, M.A. Pimenta (UFMG) and A.G. Souza Filho (UFC) for discussions about double resonance theory.

References

- [1] Ferrari AC, Robertson J. Resonant Raman spectroscopy of disordered, amorphous, and diamond-like carbon. *Phys Rev B* 2001;64:075414-1–075414-13.

- [2] Ferrari AC, Robertson J. Interpretation of Raman spectra of disordered and amorphous carbon. *Phys Rev B* 2000;61:14095–107.
- [3] Brar VW, Samsonidze GG, Dresselhaus G, Dresselhaus MS, Saito R, Swan AK, et al. Second-order harmonic and combination modes in graphite, single-wall carbon nanotube bundles, and isolated single-wall carbon nanotubes. *Phys Rev B* 2002;66:155418–27.
- [4] Huang W, Wang Y, Luo G, Wei F. 99.9% Purity multi-walled carbon nanotubes by vacuum high-temperature annealing. *Carbon* 2003;41:2585–90.
- [5] Park YS, Choi YC, Kim KS, Chung DC, Bae DJ, An KH, et al. High yield purification of multiwalled carbon nanotubes by selective oxidation during thermal annealing. *Carbon* 2001;39:655–61.
- [6] Wang Z, Huang X, Xue R, Chen L. Dispersion effects of Raman lines in carbon. *J Appl Phys* 1998;84:227–31.
- [7] Beltn T, Epron F. Characterization methods of carbon nanotubes: a review. *Mat Sci Eng B* 2005;119:105–18.
- [8] Nemanich RJ, Solin SA. First- and second-order Raman scattering from finite size crystals of graphite. *Phys Rev B* 1979;20:392–401.
- [9] Tan PH, An L, Liu LQ, Guo ZX, Czerw R, Carrol DL, et al. Probing the phonon dispersion relations of graphite from the double-resonance process of Stokes and anti Stokes Raman scatterings in multiwalled carbon nanotubes. *Phys Rev B* 2002;66:245410-1–0-8.
- [10] Kawashima Y, Katagiri G. Fundamentals, overtones and combinations in Raman spectrum of graphite. *Phys Rev B* 1995;52:10053–9.
- [11] Mennella V, Monaco G, Colangeli L, Bussoletti E. Raman spectra of carbon based materials. *Carbon* 1995;33:115–21.
- [12] Vidano RP, Fischbach DB, Willis LJ, Loehr TM. Observation of Raman band shifting with excitation wavelength for carbons and graphites. *Solid State Commun* 1981;39:341–4.
- [13] Pocsik I, Hundhausen M, Koos M, Ley L. Origin of the D peak in the Raman spectrum of microcrystalline graphite. *J Non Cryst Solids* 1998;230:1083–6.
- [14] Sood AK, Gupta R, Asher S. Origin of the unusual dependence of Raman D band on excitation wavelength in graphite-like materials. *J Appl Phys* 2001;90:4494–7.
- [15] Piscanec S, Lazzeri M, Mauri F, Ferrari AC, Robertson J. Kohn anomalies and electron–phonon interactions in graphite. *Phys Rev Lett* 2004;93:185503.1–3.4.
- [16] Li W, Zhang H, Wang C, Zhang Y, Xu L, Zhu K, et al. Raman characterization of aligned carbon nanotubes produced by thermal decomposition of hydrocarbon vapor. *Appl Phys Lett* 1997;70:2684–6.
- [17] Baranov AV, Bekhterev AN, Bobovich YS, Petrov VI. Interpretation of certain characteristics in Raman spectra of graphite and glassy carbon. *Opt Spectrosc* 1987;62:612–6.
- [18] Saito R, Grüneis A, Samsonidze GG, Brar VW, Dresselhaus G, Dresselhaus MS, et al. Double resonance Raman spectroscopy of single-wall carbon nanotubes. *New J Phys* 2003;5:157.1–157.15.
- [19] Thomsen C, Reich S. Double resonant Raman scattering in graphite. *Phys Rev Lett* 2000;85:5214–7.
- [20] Grüneis A, Saito R, Kimura T, Cançado LG, Pimenta MA, Jorio A, et al. Determination of two-dimensional phonon dispersion relation of graphite by Raman spectroscopy. *Phys Rev B* 2002;65:155405-1–5-7.
- [21] Saito R, Jorio A, Souza Filho AG, Grueneis A, Pimenta MA, Dresselhaus G, et al. *Physica B* 2002;323:100–6.
- [22] Saito R, Jorio A, Souza Filho AG, Dresselhaus G, Dresselhaus MS, Pimenta MA. Probing phonon dispersion relations of graphite by double resonance Raman scattering. *Phys Rev Lett* 2002;88(2):027401-1–4.
- [23] Moshkalyov AS, Moreau ALD, Gutterierrez HR, Cotta MA, Swart JW. Carbon nanotubes growth by chemical vapor deposition using thin film nickel catalyst. *Mater Sci Eng B* 2004;112:147–53.
- [24] Dresselhaus MS, Dresselhaus G, Saito R, Jorio A. Raman spectroscopy of carbon nanotubes. *Phys Report* 2005;409:47–99.
- [25] Choi S, Park KH, Lee S, Koh KH. Raman spectra of nano-structured carbon films synthesized using ammonia-containing feed gas. *J Appl Phys* 2002;92:4007–11.
- [26] Reich S, Thomsem C. Raman spectroscopy of graphite. *Phil Trans Roy Soc A* 2004;362:2271–88.
- [27] Lee YJ. The second order Raman spectroscopy in carbon crystallinity. *J Nucl Mater* 2004;325:174–9.
- [28] Castiglioni C, Mapelli C, Negri F. Origin of the D line in the Raman spectrum of graphite: a study based on Raman frequencies and intensities of polycyclic aromatic hydrocarbon molecules. *J Chem Phys* 2001;114:963–74.
- [29] Tuinstra F, Koenig JL. Raman spectrum of graphite. *J Chem Fis* 1970;53:1126–32.
- [30] Tan PH, Hu CY, Dong J, Shen WC, Zhang BF. Polarization properties, higher-order Raman spectra, and frequency asymmetry between Stokes and anti-Stokes scattering of Raman modes in a graphite whisker. *Phys Rev B* 2001;64:214301-1–214301-12.
- [31] Barros EB, Demir NS, Souza Filho AG, Mendes Filho J, Jorio A, Dresselhaus G, et al. Raman spectroscopy of graphitic foams. *Phys Rev B* 2005;71:165422-1–2-5.
- [32] Tan PH, Dimovski S, Gogotsi Y. Raman scattering of non-planar graphite: arched edges, polyhedral crystals, whiskers and cones. *Phil Trans Roy Soc A* 2004;362:2289–310.
- [33] Compagnini G, Puglisi O, Foti G. Raman spectra of virgin and damaged graphite edge planes. *Carbon* 1997;35:1793–7.
- [34] Tan PH, Deng YM, Zhao Q. Temperature-dependent Raman spectra and anomalous Raman phenomenon of highly oriented pyrolytic graphite. *Phys Rev B* 1998;58:5435–9.
- [35] Shimada T, Sugai T, Fantini C, Souza M, Cançado LG, Jorio A, et al. Origin of the 2450 cm^{-1} Raman bands in HOPG, single-wall and double-wall carbon nanotubes. *Carbon* 2005;43:1049–54.
- [36] Gogotsi Y, Libera JÁ, Kalashnikov N, Yoshimura M. Graphite polyhedral crystals. *Science* 2000;290:317–20.
- [37] Dong J, Shen W, Tatarchuck B. Origin of strong G' band in Raman spectra of carbon whiskers. *Appl Phys Lett* 2002;80:3733–5.